Elevated Copper Binding Strength of Amyloid-β Aggregates Enables Their Copper Sequestration from Albumin: a Pathway to Accumulation of Copper in Senile Plaques

Dianlu Jiang[a,#], *Lin Zhang*[a,#], *Gian Paola G. Grant*[a], *Christopher G. Dudzik*[b], *Shu Chen*[a], *Sveti Patel*[a], *Yuanqiang Hao*[a], *Glenn L. Millhauser*[b], *and Feimeng Zhou*[a,*]

[a]: Department of Chemistry and Biochemistry, California State University, Los Angeles, Los Angeles, California 90032

[b]: Department of Chemistry and Biochemistry, University of California, Santa Cruz, Santa Cruz, California 95064

Summary of reported binding affinities of Aβ peptides. The measured binding affinities of Aβ scatter across an extremely wide range in literature (Table S1). In early reports, usually the reported affinity constants were not corrected for the buffer effect and many other experimental factors, hence the reported K_d values are higher (although Bush and coworkers reported an attomolar K_d value,[1] an exceedingly small value). In recent years, the reported values are usually corrected for the buffer effect and more carefully measured by taking into considerations of the detection and sample pretreatment methods. The buffer-corrected K_d values are now confined within a much narrower range (typically from nM to sub-nM; although the study by Sarell et al.[2] reported a K_d value of 60 pM for the Aβ(1−42) monomer). We also contrasted in Table S1 the methods to deduce the K_d values and the sample pretreatment protocols. As can be seen, essentially all of the fluorescence-based measurements rely on the determination of the intrinsic fluorescence of the sole Tyr residue at position 10 of the various Aβ peptides. Also notice that HEPES is the most commonly employed buffer given its low Cu(II) binding strength.

Table S1. Binding constants of representative Aβ peptides and methods used

Peptide	K_d	pH	Buffer	Method	Pretreatment	ref.
Aβ(1–16)	1.0 μM (71 nM)[a]	7.4	10 mM PBS	Direct Tyr. fl.	n/a	3
Aβ(1–16)	0.4 μM (28 nM)[a]	7.4	10 mM PBS	Competitive Tyr fl.	n/a	3
Aβ(1–16)	~ 0.3 nM	7.4	20 mM PIPES	ITC	Water, centrifuged	4
Aβ(1–16)	0.1 μM	7.8	Water	Competitive Tyr fl.	n/a	5
Aβ(1–16)	0.7 nM	7.2	20 mM HEPES	ITC	n/a	6
Aβ(1–16)	47 μM (54 nM)[a]	7.4	100 mM Tris	Direct Tyr fl.	n/a	7
Aβ(1–16)	0.3 nM	7.4	20 mM HEPES	ITC	n/a	8
Aβ(1–16)	0.3 nM	7.4	20 mM PIPES	ITC	n/a	8
Aβ(1–16)	0.09/0.1 μM	7.4	50 mM HEPES	ITC/direct and competitive Tyr fl.	n/a	9
Aβ(1–28)	23 μM (1.7 nM)[b]	7.4	20 mM ACES	ITC	n/a	10
Aβ(1–28)	70 nM	7.4	50 mM HEPES	ITC	n/a	9
Aβ(1–28)	10-100 nM	7.8	Water	CD/Competitive Tyr. fl.	n/a	11
Aβ(1–28)	110 pM	7.6	Water	CD	n/a	2
Aβ(1–28)	28 μM (32 nM)[b]	7.5	100 mM Tris	Direct Tyr fl.	HFIP	7
Aβ(1–28)	2.5 μM (77 nM)[b]	7.2	10 mM HEPES	Competitive Tyr fl.	NaOH	12
Aβ(1–40)	0.9 μM (24 nM)[b]	7.4	50 mM HEPES	Direct Tyr fl.	HFIP	13
Aβ(1–40)	0.5 μM (13 nM)[b]	7.4	50 mM HEPES	Competitive Tyr fl.	HFIP	13
Aβ(1–40)	1.6 μM (73 nM)[b]	7.4	10 mM Tris	Direct Tyr fl.	n/a	14
Aβ(1–40)	~ 0.5 nM	7.4	20 mM PIPES	ITC	NaOH, centrifuged	4
Aβ(1–40)	11 μM (12 nM)[b]	7.5	100 mM Tris	Direct Tyr fl.	HFIP	7
Aβ(1–40)	1.6 μM	7.3	5 mM Phosphate buffer	NMR	n/a	15
Aβ(1–40)	8 μM (120 nM)[b]	7.4	50 mM PBS	Direct Tyr fl.	n/a	16
Aβ(1–40)	0.4 nM	7.4	20 mM HEPES	ITC	NaOH, centrifuged	8
Aβ(1–40)	1.1 nM	7.2	20 mM PIPES	ITC	NaOH, centrifuged	8
Aβ(1–40)	5 nM	7.4	20 mM Tris	CMCA	Water, centrifuged	1
Aβ(1–40)	57 nM[b]	7.4	50 mM HEPES	Tyr fl.	n/a	17
Aβ(1–42)	6-60 pM	7.4	Water	Competitive Tyr fl.	In NaOH, rocked for 48 h	2
Aβ(1–42)	0.7 μM (50 nM)[a]	7.4	10 mM PBS	Direct Tyr.fl.	NaOH	3
Aβ(1–42)	2 μM (91 nM)[b]	7.4	10 mM Tris	Direct Tyr fl.	n/a	14
Aβ(1–42)	0.007 pM	7.4	20 mM Tris	CMCA	Water, centrifuged	1
Aβ(1–42)	0.76 μM (48 nM) [b]	7.4	20 mM HEPES	Direct Tyr fl.	HFIP	13

a: K_d corrected by us with the eq. S2
b: K_d corrected by references (18 and 19)
ACES: *N*-(2-Acetamido)-2-aminoethanesulfonic acid); PIPES: piperazine-*N,N*'-bis(2-ethanesulfonic acid); Tris: tris(hydroxymethyl)aminomethane.
fl: Fluorescence; ITC: isothermo titration calorimetry (ITC); CD: Circular Dichroism; CMC: Competitive metal capture analysis

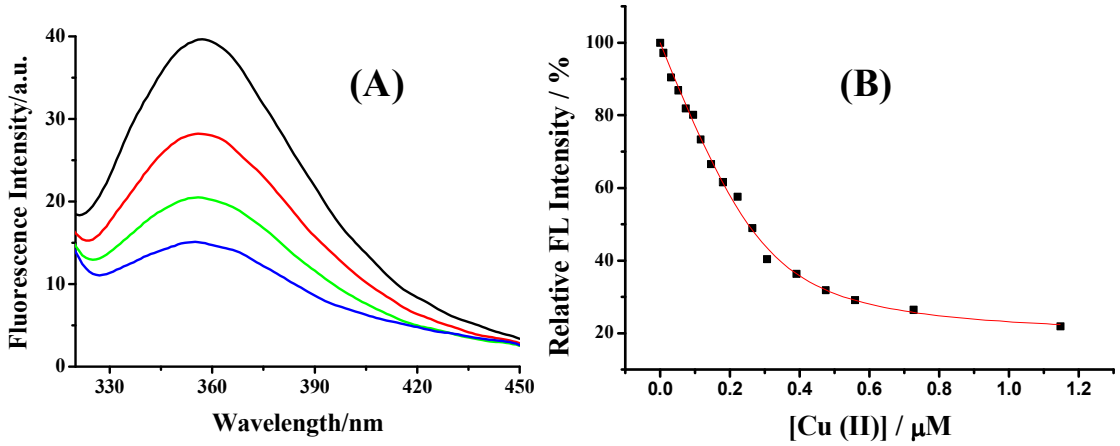

Figure S1. (A) Fluorescence emission spectra of 0.5 μM Aβ(1–16)(Y10W) probe without (black curve) and with addition of Cu(II) at different concentrations: 0.20 (red curve), 0.30 (green curve), and 0.47 μM (blue curve). (B) The relative fluorescence intensity (solid squares) and the fitted curve (red line) against Cu(II) concentration in 500 mM HEPES buffer (pH 7.4).

Determination of the copper binding constant of the probe. To determine the apparent binding constant of Aβ(1–16)(Y10W) at different aggregation times, the Cu(II) binding constant of the Aβ(1–42) probe was measured first. Figure S1A shows the fluorescence spectra of the probe when titrated with Cu(II). The fluorescence intensity decreases with increasing Cu(II) concentrations, showing a behavior identical to that of Aβ(1–16) or Aβ(1–42).[3, 11] The fluorescence of Aβ(1–16)(Y10W) is over five times stronger than that of Aβ(1–16) (see also Figure S10), allowing a more accurate binding constant to be measured. Shown in Fig. S1B are the relative fluorescence intensity (solid squares) at 360 nm and the fitted curve (red curve) against the amount of Cu(II) titrant. The change of the probe fluorescence upon Cu(II) binding correlates well with the amount of Aβ(1–

16)(Y10W)–Cu(II) complex formed. Thus, the apparent binding constant, K'_{app}, of Aβ(1–16)(Y10W)–Cu(II) can be determined from the fluorescence intensity as a function of the total Cu(II) concentration, [L], using eq. S1.[3, 20]

$$\Delta F = F_0 - F_L = \frac{F_0 - F_\infty}{2[M_0]}[([L]+[M_0]+\frac{1}{K'_{app}}) - (([L]+[M_0]+\frac{1}{K'_{app}})^2 - 4[M_0][L])^{1/2}] \qquad \text{(S1)}$$

where F_0 and F_L are the fluorescence intensities of the probe in the absence and presence of $CuCl_2$, respectively. F_∞ is the fluorescence intensity of a solution in which the probe is saturated with $CuCl_2$ and no further quenching occurs. $[M_0]$ is the concentration of the probe binding site, taken to be equal to the Aβ(1–16)(Y10W) concentration, as it is commonly known that under most circumstances Cu(II) forms a 1:1 complex with monomeric Aβ *in vitro*. From the fit, K_{app} of Aβ(1–16)(Y10W) to Cu(II) was determined be 7.5×10^6 M^{-1} in 500 mM HEPES buffer or 1.7×10^6 M^{-1} in 10 mM phosphate buffer. The K_{app} value of Aβ(1–16)(Y10W) in the phosphate buffer is highly comparable to our previously reported values for Aβ(1–42) (1.4×10^6 M^{-1}) and Aβ(1–16) (1.0×10^6 M^{-1}) under the same condition.[3] The similar binding strengths suggest that Cu(II) would be equally allocated between the Aβ(1–16)(Y10W) probe and monomeric Aβ(1–42).

To measure the probe binding constant more accurately we used a high concentration of HEPES (500 mM) and a low probe concentration for titration so that buffer would compete with the probe for copper.[21] Under the condition that the HEPES concentration is six orders of magnitude greater than the Aβ(1–16)(Y10W) concentration, the buffer effect[21] needs to be corrected. The binding constant K' (reciprocal of dissociation constant K_d) is corrected with the following equation, with the C term known at a given buffer concentration:[22]

$$\log K' = \log K_{app} + C \quad \text{(S2)}$$

In this work, the only time when the HEPES buffer effect is important is for the measurement of the Cu(II) binding affinity constant (i.e., the case shown in Figure S1). This is because the measurement is more accurate when the probe concentration is closer to the dissociation constant of its Cu(II) complex. An even lower probe concentration would be better, but the fluorescence signal becomes difficult to detect. The K_{app} value of 7.5×10^6 M^{-1} detected in 500 mM HEPES was corrected to be 3.1×10^9 M^{-1} using eq S2.

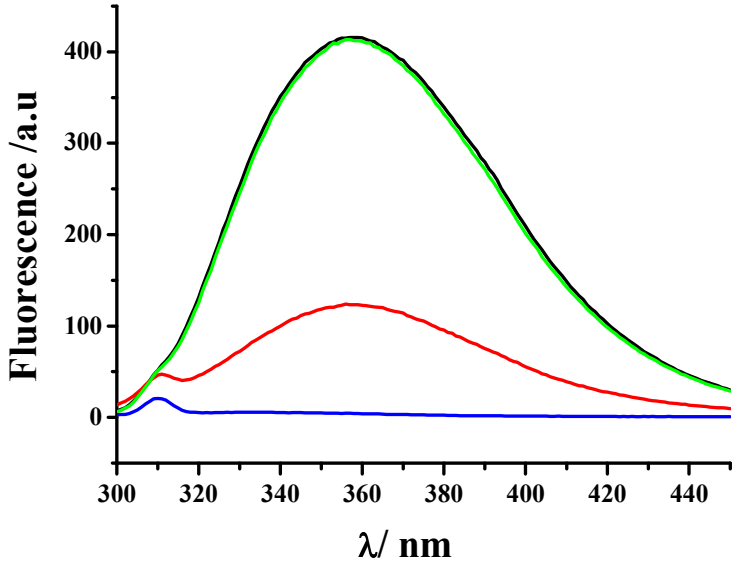

Figure S2. Fluorescence spectra collected from 10 mM HEPES buffer (blue curve), 12.5 μM Aβ(1−16)(Y10W) in 10 mM HEPES (black), a mixture of 12.5 μM Aβ(1−16)(Y10W) and 12.5 μM Cu(II) (red), and a mixture containing 12.5 μM each of Aβ(1−16)(Y10W), Cu(II), and EDTA (green).

Removal of Cu(II) in the Aβ(1–16)(Y10W)–Cu(II) complex by a stronger copper chelator (EDTA) fully recovers the fluorescence. Figure S2 shows an overlay of

fluorescence spectra collected from 10 mM HEPES buffer (blue curve) and 12.5 μM Aβ(1−16)(Y10W) in 10 mM HEPES buffer (black). In the HEPE buffer, only the water Raman peak was observed at 313 nm (vide infra), whereas the Aβ(1−16)(Y10W) probe exhibits an emission peak at 360 nm. Addition of Cu(II) significantly decreases the probe fluorescence. In the mixture comprising Aβ(1−16)(Y10W), Cu(II), and EDTA (12.5 μM each), the fluorescence intensity is the same as that of the Aβ(1−16)(Y10W)-only solution. Therefore, in the presence of a stronger Cu(II) chelator, Cu(II) bound by Aβ(1−16)(Y10W) can be completely removed, demonstrating that Aβ(1−16)(Y10W) can serve as an excellent probe to report on Cu(II) sequestration by Aβ(1−42) monomers and aggregates.

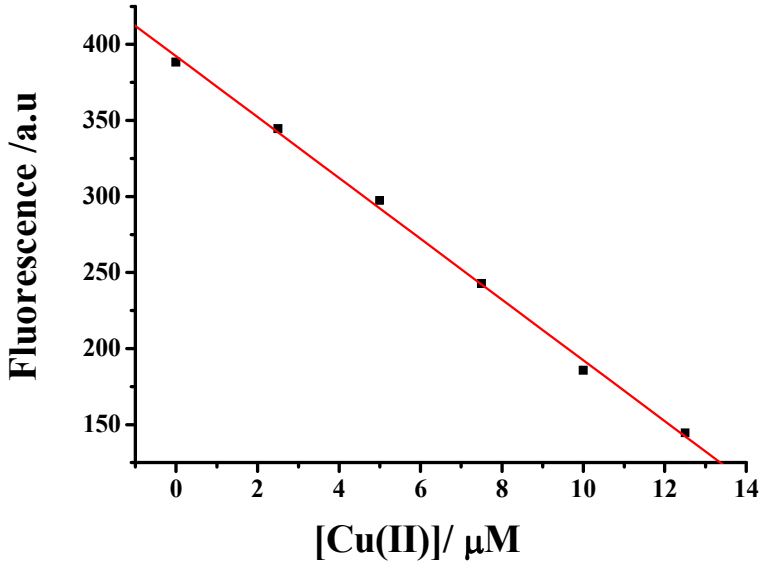

Figure S3. Titration of 12.5 μM Aβ(1−16)(Y10W) with Cu(II) in 10 mM HEPES (R^2 = 0.995).

Buffer effect on the binding constant measurement. HEPES is usually regarded as a weak ligand to copper with a binding constant of 1.6×10^3 M^{-1}.[8, 21, 23] Such a value is much

lower than that of Aβ(1–16)(Y10W) or Aβ(1–42). The effect of HEPES on the measurement of the Cu(II) binding constant of the Aβ(1–16)(Y10W) probe is not significant even when the HEPES concentration is three orders of magnitude greater than that of the probe. At the concentration used for all of the fluorescence competitive assays presented in the main text (10 mM), HEPES is simply a spectator compound. Indeed, the fluorescence signal of 12.5 μM Aβ(1–16)(Y10W) in 10 mM HEPES exhibits a linear decrease versus the amount of Cu(II) up to one equivalent (Figure S3). The linear relationship confirms that Cu(II) titrated into this solution is essentially all bound to the probe. Furthermore, in the competitive assays, the total ligand concentration, [Aβ(1–16)(Y10W)] + [Aβ(1–42)], is more than twice as high as the total Cu(II) concentration. Consequently, little Cu(II) remain in solution for binding with HEPES.

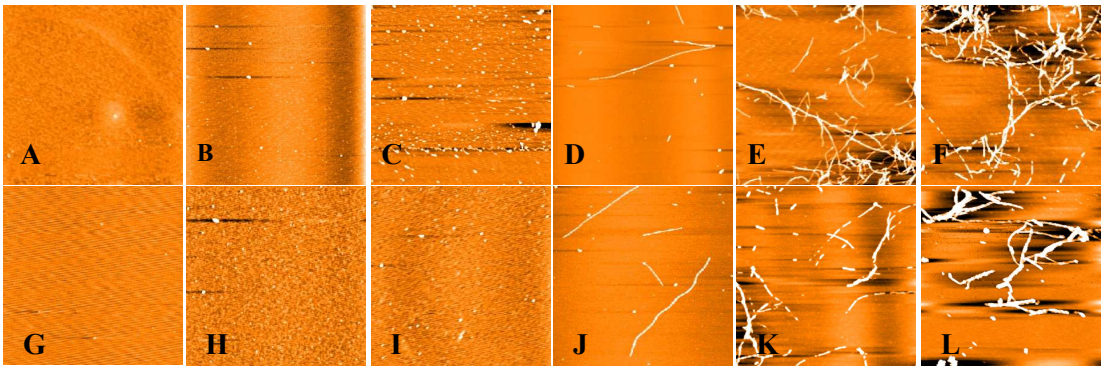

Figure S4. AFM images of an incubated 12.5 μM Aβ(1–42) solution (top row) and 12.5 μM Aβ(1–42) co-incubated with equimolar Aβ(1–16)(Y10W) (bottom row). These incubations were carried out at 37 °C and aliquots were withdrawn at 0, 20, 50, 180, 1440 and 2880 min and cast onto mica sheets. The image areas are all 5 μm × 5 μm.

The morphologies of Aβ(1–42) incubated in the presence and absence of Aβ(1–16)(Y10W). Juxtaposed in Figure S4 are AFM images sampled at different times from an incubated Aβ(1–42) solution (top row) and those from an Aβ(1–42) solution co-incubated with Aβ(1–16)(Y10W) (bottom row). Apparently the Aβ(1–16)(Y10W) probe does not affect the aggregation pathway and kinetics of Aβ(1–42).

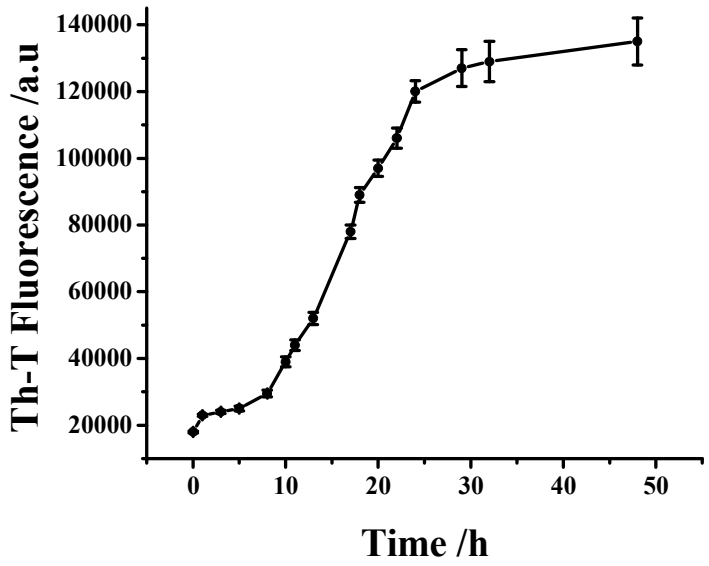

Figure S5. Aβ(1–42) aggregation monitored with the ThT assay. At different incubation times, 80 μL of 12.5 μM Aβ(1–42) was withdrawn and mixed with 320 μL of a 10 mM HEPES buffer (pH 7.4) solution containing 20 μM ThT. Fluorescence signals were measured using a Fluorolog 3 spectrofluorometer (Horiba Jobin Yvon, Edison, NJ) with slit widths of 2 nm and excitation and emission wavelengths at 450 and 480 nm, respectively. Each data point is the average of three replicate measurements.

Thioflavin-T (ThT) assay. The fibrillation process of Aβ(1−42) was monitored with the ThT assay (Figure S5). The trend is similar to those shown by other studies[24, 25] and a recent work by us[26]. The presence of a lag phase is indicative of a lack of aggregation-initiating nuclei (relatively large structural oligomers or "aggregation units") in the early stage of the Aβ(1−42) incubation, confirming that the HFIP-treated Aβ(1−42) sample contains only monomers. Notice that the plateau in Figure S5 (ca. 24 h) is consistent with the time when fibrils were observed by AFM (cf. the inset of Figure 2 at 1440 min). The trend depicted in Figure S5 is in contrast to that in Figure 2, which displays an increase of the *K* value even at 20 min from the inception of the incubation. This difference again suggests that low-mass oligomers (which are too small to serve as nuclei) bind more strongly than the Aβ(1−42) monomer.

Derivation of the apparent Cu(II) binding constant of a mixture of aggregates. All of the Aβ(1–42) aggregates are capable of binding Cu(II). We therefore define the apparent binding affinity constant (*K*) of an aggregate mixture by using the formal concentration of the Aβ(1–42) monomer. This *K* value can be derived from changes in the fluorescence intensity of the probe-Cu(II) complex at different aggregation times (states).

$$\mathrm{A\beta(1-42)+Cu(II)} \overset{K}{\longleftrightarrow} \mathrm{A\beta(1-42)-Cu(II)} \qquad \text{(S3; eq. 1 in the main text)}$$

$$\mathrm{A\beta(1-16)(Y10W)+Cu(II)} \overset{K'}{\longleftrightarrow} \mathrm{A\beta(1-16)(Y10W)-Cu(II)} \qquad \text{(S4; eq. 2 in the main text)}$$

$$K = \frac{[\mathrm{A\beta(1-42)-Cu(II)}]}{[\mathrm{A\beta(1-42)}][\mathrm{Cu(II)}]} \qquad \text{(S5)}$$

$$K' = \frac{[\mathrm{A\beta(1-16)(Y10W)-Cu(II)}]}{[\mathrm{A\beta(1-16)(Y10W)}][\mathrm{Cu(II)}]} \qquad \text{(S6)}$$

K changes with the aggregation time, but K' remains constant because Aβ(1−16)(Y10W) does not aggregate. Let θ_w be the percentage of Cu(II)-binding Aβ(1–16)Y10W and θ be the percentage of Cu(II)-binding Aβ(1–42), then:

$$\theta = \frac{K[\mathrm{Cu(II)}]}{1 + K[\mathrm{Cu(II)}]} \qquad \text{(S7)}$$

and $$\theta_w = \frac{K'[\mathrm{Cu(II)}]}{1 + K'[\mathrm{Cu(II)}]} \qquad \text{(S8)}$$

Mass balance leads to the following equation:

$$[\mathrm{Cu(II)}] + [\mathrm{A\beta(1–16)(Y10W)–Cu(II)}] + [\mathrm{A\beta(1–42)–Cu(II)}] = [\mathrm{Cu(II)}]_T \qquad \text{(S9)}$$

where $[\mathrm{Cu(II)}]_T$ represents the total Cu(II) concentration. In eq. S9, Cu(II) bound by HEPES is neglected because the amount of Cu(II) complex of HEPES is insignificant (vide supra).

Solving for [Cu(II)], the following can be derived:

$$[\mathrm{Cu(II)}] = \frac{\theta_w}{K'(1-\theta_w)} \qquad \text{(S10)}$$

Plugging eq. S10 into eq. S7, θ can be solved:

$$\theta = \frac{K[\mathrm{Cu(II)}]}{1 + K[\mathrm{Cu(II)}]} = \frac{K\dfrac{\theta_w}{K'(1-\theta_w)}}{1 + K\dfrac{\theta_w}{K'(1-\theta_w)}} = \frac{K\theta_w}{K'(1-\theta_w) + K\theta_w} \qquad \text{(S11)}$$

Letting the initial concentrations of Aβ(1–42) and Aβ(1−16)(Y10W), and the total concentration of Cu(II) be A, L_0 and C, respectively, and substituting these terms into eq. S9 gives

$$\frac{\theta_w}{K'(1-\theta_w)} + \theta_w L_0 + A\frac{K\theta_w}{K'(1-\theta_w) + K\theta_w} = C \qquad \text{(S12)}$$

K therefore can be obtained by rearranging eq. S12:

$$K = \frac{\left[K'(1-\theta_w)(C-\theta_w L_0)-\theta_w\right](1-\theta_w)K'}{K'A\theta_w(1-\theta_w)-\theta_w\left[K'(1-\theta_w)(C-\theta_w L_0)-\theta_w\right]} \qquad \text{(S13; eq. 3 in the main text)}$$

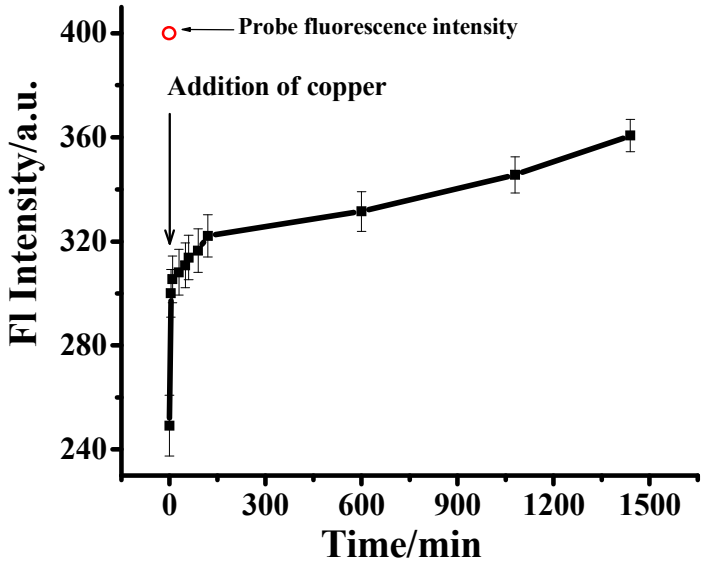

Figure S6. Recovery of the Aβ(1–16)(Y10W) fluorescence monitored continuously in a single solution of Aβ(1–42), Aβ(1–16)(Y10W), and Cu(II) while being incubated in a quartz cuvette. The concentration of Cu(II), Aβ(1–42) and Aβ(1–16)(Y10W) was all 12.5 μM. Each data point is the average of three replicate measurements. The empty red circle corresponds to the fluorescence signal in a mixture of 12.5 μM Aβ(1–16)(Y10W) and 12.5 μM Aβ(1–42).

Continuous fluorescence monitoring of a single solution of Aβ(1–16)(Y10W), Cu(II), and Aβ(1–42). Instead of making multiple solutions by mixing the Aβ(1–16)(Y10W) probe with aliquots withdrawn from a continuously incubated Cu(II)/Aβ(1–42) solution (i.e., the experiment shown by Figure 4), the probe fluorescence variation can be continuously monitored in a single solution that also contains Aβ(1–42) and Cu(II).

Specifically, into a cuvette containing 400 µL of 12.5 µM Aβ(1−16)(Y10W) and 12.5 µM Aβ(1−42), 10 µL of 500 µM Cu(II) was spiked. As shown in Figure S6, immediately after the addition of Cu(II), the probe fluorescence was quenched from the level denoted by the red circle to a much lower level (ca. 250). The quenched fluorescence was recovered to almost 30% of the initially quenched value within the first 10 min, suggesting that a rapid redistribution of Cu(II) between the probe and Aβ(1−42) had been established. Thereafter, the fluorescence signal increases more gradually as the Aβ(1−42) oligomerization and fibrillation occurs. At 24 h or 1440 min, the fluorescence recovered to about 80% of the initially quenched value. This coincides with the time when fibrils appear in solution (cf. Figure 2A and the inset). Beyond 24 h, the fluorescence signal begins to fluctuate due to the light scattering by fibrils and large aggregates (see also description in the main text).

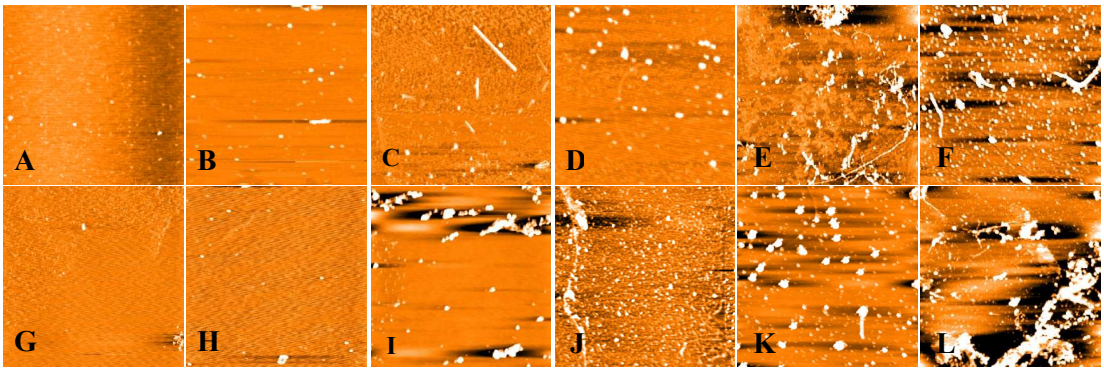

Figure S7. AFM images of 12.5 µM Aβ(1−42) co-incubated with equimolar Cu(II) (top row) and with equimolar amounts of Aβ(1−16)(Y10W) and Cu(II) (bottom row). The incubation temperature was 37 °C and aliquots were withdrawn at 0, 20, 50, 180, 1440 and 2880 min. The image areas are all 5 µm × 5 µm.

The morphologies of Aβ(1–42) incubated in the presence and absence of Aβ(1–16)(Y10W) and Cu(II). Figure S7 displays AFM images of Aβ(1–42) co-incubated with Cu(II) (top row) and Aβ (1–42) co-incubated with Aβ(1–16)(Y10W) and Cu(II) (bottom row). The presence of copper leads to amorphous aggregate formation. Compared to Figure 4 in the main text, it is evident that Aβ(1–16)(Y10W) does not change the Aβ(1–42) aggregation pathways and kinetics.

Determination of the copper binding constant (*K*) of aggregated Aβ(1–42) by competitive EPR binding assay. For a competitive EPR binding assay to be successful, the two Cu(II) competing ligands should not have drastically different binding constants. Moreover, ideally their main EPR peaks and/or hyperfine peaks should be at different positions so that quantitative measurements of the Cu(II) transfer can be made. We attempted to observe possible transfer between Aβ(1–42) aggregates and a number of copper binding molecules (e.g., nitrilotriacetic acid, the oxidized form of glutathione, a pentapeptide of sequence Ac-GGGGG, and α-synuclein) and found that they do not behave as well as the HSA–Cu(II) system, which is also the most biologically relevant source of copper among all of the species we studied.

We estimated the copper binding constant (*K*) of aggregated Aβ(1–42) by deconvoluting the two components in curve D (cf. Figure 5 in the main text) to yield a ratio of Cu(II) bound to HSA versus that complexed by the Aβ(1–42) aggregates. In all cases, Cu(II) and HSA concentrations were 49 and 61 μM, respectively. Such a competitive assay was successfully applied by Millhauser and coworkers to studies of copper binding by peptides derived from the prion protein sequence.[27] Relative to HSA

whose copper binding constant is 1×10^{12} M^{-1}, [22] the estimated *K* value of pre-incubated Aβ (from curve D) is 1.7×10^{11} M^{-1}, which is in good agreement with the value deduced from our fluorescence measurement (0.8×10^{11} M^{-1}). In contrast, the *K* value of monomeric Aβ(1–42) estimated from curve B is 1.1×10^{10} M^{-1}, a value one order of magnitude smaller than that of the Aβ(1–42) aggregates and three times smaller than that obtained from our fluorescence method. It is important to note that the actual *K* of a freshly prepared Aβ(1–42) at the higher Aβ(1–42) concentration necessary for EPR might be overestimated, owing to the increased propensity to form oligomers in a more concentrated solution. In addition, inevitably there is also some delay between the sample preparation and the EPR measurement, which could also lead to formation of a small amount of soluble Aβ(1–42) oligomers (i.e., similar to those identified by the red curve in Figure 3). We should also mention that the accuracy of the binding constant value estimated from the EPR measurements is also dependent on the extent of dispersion of the copper-containing Aβ(1–42) aggregates inside the EPR tubes. As incubation prolongs, more aggregates are formed and the likelihood their sedimentation out of the EPR detection window increases. Indeed we observed that the loss of the total copper signal is more pronounced at longer Aβ(1–42) incubation times. An underestimate of the *K* values is expected for Aβ(1–42) samples incubated for 6 h or longer due to precipitation. Nevertheless, both the EPR spectra shown in Figure 4 and the binding constants estimated from the competitive EPR assay (cf. Table S2) have unequivocally validated the increased binding affinity associated with aggregated Aβ(1–42).

Table S2. Cu(II) binding constants of Aβ(1–42) estimated from competitive assays

Aβ (1–42) concentration (μM)	Incubation time at 37 °C (h)	$K \times 10^{10}$ M^{-1}
76	0	3.3
76	6	22.7
76	24	16.4
306	0	2.2
306	6	20.0
306	24	22.7

Comparative studies of Aβ(1–42) samples treated with different protocols. Aβ(1–42) is prone to aggregation, and care should be taken to eliminate oligomers or seeds that can accelerate the aggregation and fibrillation processes in the early stage of an incubation or during titration. Different methods have been developed to treat commercial or homemade Aβ(1–42) samples. As shown in Table S1, most studies resort to the method developed by Teplow and coworkers[28] or the method of dissolving preexisting oligomers with HFIP followed by removal of insoluble particles.[7, 18] We noticed that the sample pretreatment method used by Sarell et al.[2] is different from all other studies and might have at least partially contributed to the rather low K_d value for the Aβ(1–42) monomer. We followed this method by shaking Aβ(1–42) stock solution at 5 ºC for 48 h and found that a large amount of oligomers (Fig. S8A) were present in the stock solution. This is in contrast to the HFIP-treated sample which showed few globular oligomers (Figure S8B). Quenching of the Tyr-10 fluorescence by Cu(II) (Figure S9A) and recovery of the quenched fluorescence by glycine (Figure S9B) are also different between samples treated with these two methods. In 10 mM HEPES and at 50 μM (a concentration much higher than the K_d values of Aβ peptides), Cu(II) is not bound by HEPES and a linear dependence of the fluorescence intensity on the Cu(II) concentration is expected (cf.

Figure S3). It is clear from Figure S9A, the data collected from an Aβ(1−16) solution (green curve) and the HFIP-treated Aβ(1−42) solution (red curve) depict better linearity than that from the Aβ(1−42) solution treated with the method of Sarell et al.[2] (black curve). The deviation from linearity can be ascribed to the presence of oligomers in the solution which accelerates the precipitation upon copper binding(cf. Figure S8A). This conclusion is further supported by the fluorescence competitive assay using glycine (a Cu(II) chelator) as a competitive ligand. As shown in Figure S9B, The half maximal quenching values obtained with the HFIP-treated Aβ(1−42) sample, Aβ(1−42) treated with the Sarell method,[2] and Aβ(1−16) are 12, 60 (which is comparable to that reported in Reference 2), and 10, respectively. It is evident that the Cu(II) binding affinity of the HFIP-treated Aβ(1−42) sample is closer to that of Aβ(1−16) than to that of the Aβ(1−42) sample treated with the method by Sarell et al. Furthermore, the quenched Aβ(1−16) fluorescence is almost completely recovered with the addition of excess glycine, while the fluorescence recovery of the HFIP-treated Aβ(1−42) is greater than that of the Aβ(1−42) sample treated with the Sarell method. That in Aβ(1−42) solutions the fluorescence signal did not fully recover can be reasoned to the presence of large aggregates formed during the titration with Cu(II) and the addition of glycine. We believe that some Cu(II)-containing aggregates may have precipitated, decreasing the Cu(II) ions available to glycine. Overall, the data presented in Figures S8 and S9 strongly suggest that sample treatment and assay methods are crucial to accurate determination of the binding constant of Aβ(1−42) aggregates.

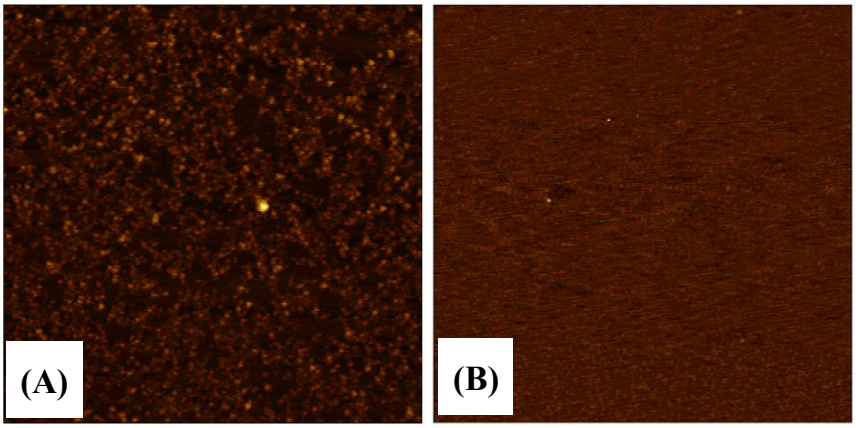

Figure S8. AFM images of Aβ(1–42) treated with the method used by Sarell et al. (A) and with HFIP (B). The image areas are both 5 μm × 5 μm.

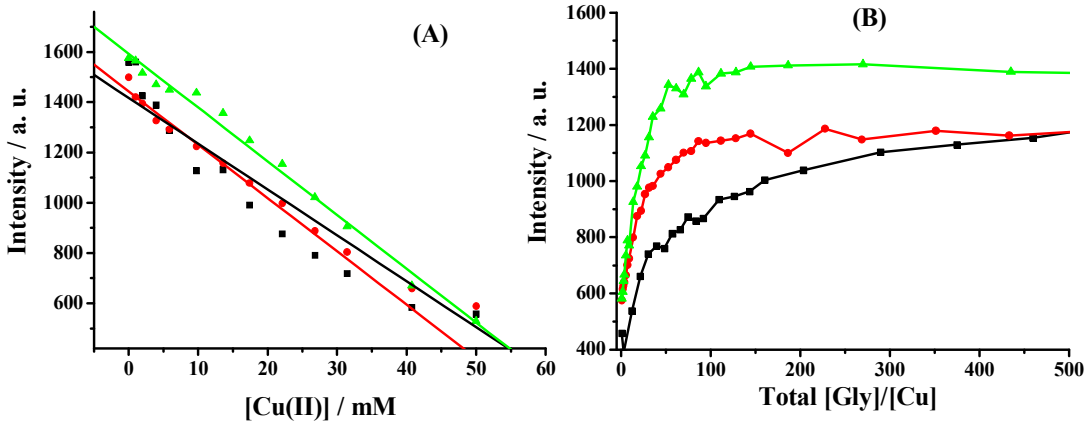

Figure S9. (A) Titrations of 50 μM Aβ(1–42) prepared from stock solutions treated with the method reported by Sarell et al. (black curve) and with the HFIP method (red) using Cu(II) as the titrant. For comparison, a 50 μM Aβ(1–16) sample was also titrated (green curve). Linear regressions of these plots yielded R^2 values of –0.995, –0.991, and –0.964, for Aβ(1–16), HFIP-treated Aβ(1–42), and Aβ(1–42) treated with the Sarell method, respectively. (B) Additions of glycine immediately after the Aβ solutions shown in (A) were titrated with Cu(II). The buffer system was 10 mM HEPES at pH 7.4 and the Tyr-10 fluorescence of these three species were monitored at 307 nm. A Hitachi 4600

spectrofluorimeter was used for the measurements with entrance and exit slit widths both set at 5 nm.

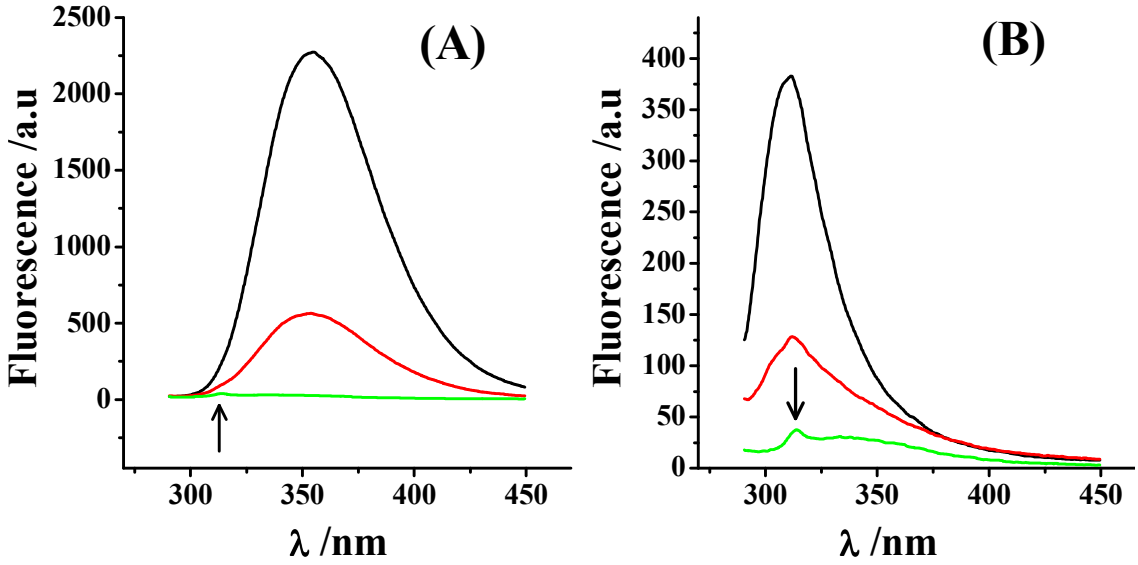

Figure S10. Fluorescence spectra of (A) 50 μM Aβ(1–16)(Y10W) and (B) 50 μM Aβ(1–42) in 10 mM HEPES: Aβ(1–16)(Y10W) or Aβ(1–42) alone (black curves) and Aβ(1–16)(Y10W) or Aβ(1–42) with one equivalent of Cu(II) added (red curves). Spectra from the buffer are shown in green. A Hitachi 4600 spectrofluorimeter was used for the measurements with entrance and exit slit widths set at 2.5 and 5 nm, respectively. The arrows indicate the water Raman peak.

Advantages of the Aβ(1–16)(Y10W) probe for binding constant measurements. The method resorting to measurements of the Try-10 fluorescence for Cu(II) binding constants suffers from the interference of the water Raman peak and low fluorescence signal. The latter is particularly pronounced when Cu(II) concentrations approach to the stoichiometric equivalent of the Aβ peptide at which the Tyr-10 fluorescence is quenched to the highest extent. As shown in Figure S10, the water Raman peak (ca. 313 nm) is in

close proximity of the Tyr fluorescence (307 nm). In contrast, the Aβ(1−16)(Y10W) probe (emission at 360 nm) is farther away from the water Raman peak. Notice that, under the same experimental condition, the Aβ(1−16)(Y10W) probe has a fluorescence intensity that is almost six times greater than the Tyr-10 of Aβ(1–42).

References:

(1) Atwood, C. S., Scarpa, R. C., Huang, X. D., Moir, R. D., Jones, W. D., Fairlie, D. P., Tanzi, R. E. and Bush, A. I. (2000) Characterization of copper interactions with Alzheimer amyloid beta peptides: identification of an attomolar-affinity copper binding site on amyloid beta 1–42. *J. Neurochem. 75*, (3), 1219–1233.

(2) Sarell, C. J., Syme, C. D., Rigby, S. E. J. and Viles, J. H. (2009) Copper(II) binding to amyloid-beta fibrils of Alzheimer's disease reveals a picomolar affinity: stoichiometry and coordination geometry are independent of Aβ oligomeric form. *Biochemistry 48*, (20), 4388–4402.

(3) Maiti, N. C., Jiang, D. L., Wain, A. J., Patel, S., Dinh, K. L. and Zhou, F. M. (2008) Mechanistic studies of Cu(II) binding to amyloid-beta peptides and the fluorescence and redox behaviors of the resulting complexes. *J. Phys. Chem. B 112*, (28), 8406–8411.

(4) Hong, L. A., Carducci, T. M., Bush, W. D., Dudzik, C. G., Millhauser, G. L. and Simon, J. D. (2010) Quantification of the Binding Properties of Cu^{2+} to the Amyloid Beta Peptide: Coordination Spheres for Human and Rat Peptides and Implication on Cu^{2+}-Induced Aggregation. *J. Phys. Chem. B. 114*, (34), 11261–11271.

(5) Ma, Q. F., Hu, J., Wu, W. H., Liu, H. D., Du, J. T., Fu, Y., Wu, Y. W., Lei, P., Zhao, Y. F. and Li, Y. M. (2006) Characterization of copper binding to the peptide amyloid-beta(1–16) associated with Alzheimer's disease. *Biopolymers 83*, (1), 20–31.

(6) Hong, L., Bush, W. D., Hatcher, L. Q. and Simon, J. (2008) Determining thermodynamic parameters from isothermal calorimetric isotherms of the binding of macromolecules to metal cations originally chelated by a weak ligand. *J. Phys. Chem. B 112*, (2), 604–611.

(7) Karr, J. W., Akintoye, H., Kaupp, L. J. and Szalai, V. A. (2005) N-terminal deletions modify the Cu^{2+} binding site in amyloid-beta. *Biochemistry 44*, (14), 5478–5487.

(8) Hatcher, L. Q., Hong, L., Bush, W. D., Carducci, T. and Simon, J. D. (2008) Quantification of the binding constant of copper(II) to the amyloid-beta peptide. *J. Phys. Chem. B 112*, (27), 8160–8164.

(9) Guilloreau, L., Damian, L., Coppel, Y., Mazarguil, H., Winterhalter, M. and Faller, P. (2006) Structural and thermodynamical properties of Cu-II amyloid-beta 16/28 complexes associated with Alzheimer's disease. *J. Biol. Inorg. Chem. 11*, (8), 1024–1038.

(10) Sacco, C., Skowronsky, R. A., Gade, S., Kenney, J. M. and Spuches, A. M. (2012) Calorimetric investigation of copper(II) binding to A beta peptides: thermodynamics of coordination plasticity. *J. Biol. Inorg. Chem. 17*, (4), 531–541.

(11) Syme, C. D., Nadal, R. C., Rigby, S. E. J. and Viles, J. H. (2004) Copper binding to the amyloid-beta (Aβ) peptide associated with Alzheimer's disease. *J. Biol. Chem. 279*, 18169–18177.

(12) Danielsson, J., Pierattelli, R., Banci, L. and Graslund, A. (2007) High-resolution NMR studies of the zinc-binding site of the Alzheimer's amyloid beta-peptide. *FEBS J. 274*, (1), 46–59.

(13) Tougu, V., Karafin, A. and Palumaa, P. (2008) Binding of zinc(II) and copper(II) to the full-length Alzheimer's amyloid-beta peptide. *J. Neurochem. 104*, (5), 1249–1259.

(14) Garzon-Rodriguez, W., Yatsimirsky, A. K. and Glabe, C. G. (1999) Binding of Zn(II), Cu(II), and Fe(II) ions to Alzheimer's A beta peptide studied by fluorescence. *Bioorg. Med. Chem. Lett. 9*, (15), 2243–2248.

(15) Hou, L. M. and Zagorski, M. G. (2006) NMR reveals anomalous copper(II) binding to the amyloid A beta peptide of Alzheimer's disease. *J. Am. Chem. Soc. 128*, (29), 9260–9261.

(16) Raman, B., Ban, T., Yamaguchi, K., Sakai, M., Kawai, T., Naiki, H. and Goto, Y. (2005) Metal ion-dependent effects of clioquinol on the fibril growth of an amyloid beta peptide. *J. Biol. Chem. 280*, (16), 16157–16162.

(17) Rozga, M., Kloniecki, M., Dadlez, M. and Bal, W. (2010) A Direct determination of the dissociation constant for the Cu(II) complex of amyloid beta 1–40 peptide. *Chem. Res. Toxicol 23*, (2), 336–340.

(18) Tougu, V., Karafin, A. and Palumaa, P. (2008) Binding of zinc(II) and copper(II) to the full-length Alzheimer's amyloid-beta peptide. *J. Neurochem. 104*, (5), 1249–1259.

(19) Zawisza, I., Rozga, M. and Bal, W. (2012) Affinity of copper and zinc ions to proteins and peptides related to neurodegenerative conditions (A beta, APP, alpha-synuclein, PrP). *Coord. Chem. Rev. 256*, (19-20), 2297–2307.

(20) Jackson, G. S., Murray, I., Hosszu, L. L. P., Gibbs, N., Waltho, J. P., Clarke, A. R. and Collinge, J. (2001) *Proc. Natl. Acad. Sci. USA 98*, 8531–8535.

(21) Faller, P. and Hureau, C. (2009) Bioinorganic chemistry of copper and zinc ions coordinated to amyloid-βpeptide. *Dalton Trans.*, 1080–1094.

(22) Bal, W., Christodoulou, J., Sadler, P. J. and Tucker, A. (1998) Multi-metal binding site of serum albumin. *J. Inorg. Biochem. 70*, (1), 33–9.

(23) Sokołowska, M. and Bal, W. (2005) Cu(II) complexation by ‘‘non-coordinating’’ N-2-hydroxyethylpiperazine-N'-2-ethanesulfonic acid (HEPES buffer). *J. Inorg. Biochem. 99*, 1653–1660.

(24) Bartolini, M., Naldi, M., Fiori, J., Valle, F., Biscarini, F., Nicolau, D. V. and Andrisano, V. (2011) Kinetic characterization of amyloid-beta 1–42 aggregation with a multimethodological approach. *Anal. Biochem. 414*, 215–225.

(25) Sanders, H. M., Lust, R. and Teller, J. K. (2009) Amyloid-beta peptide Aβp3–42 affects early aggregation of full-length Aβ1–42. *Peptides 30*, 849–854.

(26) Jiang, D., Rauda, I., Han, S., Chen, S. and Zhou, F. (2012) Aggregation Pathways of the Amyloid β(1–42) Peptide Depend on Its Colloidal Stability and Ordered β-Sheet Stacking. *Langmuir 28* 12711–12721.

(27) Dudzik, C. G., Walter, E. D. and Millhauser, G. L. (2011) Coordination features and affinity of the Cu^{2+} site in the α-synuclein protein of Parkinson's Disease. *Biochemistry 50*, 1771–1777.

(28) Fezoui, Y., Hartley, D. M., Harper, J. D., Khurana, R., Walsh, D. M., Condron, M. M., Selkoe, D. J., Lansbury, P. T., Jr, Fink, A. L. and Teplow, D. B. (2000) An improved method of preparing the amyloid β-protein for fibrillogenesis and neurotoxicity experiments *Amyloid: Int. J. Exp. Clin. Invest. 7*, 166– 178.